

Electronic structure of thin MoS<sub>2</sub> films†Cite this: *RSC Appl. Interfaces*, 2024, **1**, 1276Benjamin A. Chambers,<sup>ab</sup> Christopher T. Gibson<sup>ab</sup> and Gunther G. Andersson \*<sup>ab</sup>Received 9th May 2024,  
Accepted 27th July 2024

DOI: 10.1039/d4lf00165f

rsc.li/RSCApplInter

The valence electron structure of exfoliated monolayer MoS<sub>2</sub> deposited onto SiO<sub>2</sub> was determined by UV photoelectron spectroscopy through component analysis in combination with Auger electron microscopy. The valence electron cut-off for bulk MoS<sub>2</sub> was found at 0.64 eV binding energy whilst monolayer MoS<sub>2</sub> and few layer MoS<sub>2</sub> have higher binding energies of 0.89 eV and 1.26 eV respectively. SiO<sub>2</sub> is known to interact only weakly with MoS<sub>2</sub>. Thus, the valence electron structure of higher binding energy determined here is thus considered to represent that of a material not affected by strain. The implications of the change in the valence electron cut-off are discussed.

## Introduction

MoS<sub>2</sub> is an example of a transition metal dichalcogenide that possesses an indirect bandgap with a transition from indirect to direct band gap when transitioning from bulk to few or monolayer thickness experimentally and through computer simulations.<sup>1–4</sup> The structure of MoS<sub>2</sub> allows fabricating monolayers through exfoliation<sup>1</sup> or growth on substrates.<sup>5–7</sup> The charges on the surface and in the bulk of MoS<sub>2</sub> are almost identical which is related to the van der Waals type bonding between layers.<sup>8</sup> The electronic and optical properties of MoS<sub>2</sub> are changing with the number of monolayers<sup>9–12</sup> and at the edges of the crystallites.<sup>13</sup> Changing the numbers of monolayers forming a sample allows for tuning its properties – also through combining with other metal dichalcogenides<sup>9</sup> – for a range of applications such as energy conversion and storage<sup>14</sup> and biomedical applications.<sup>15</sup> A challenge in using monolayer MoS<sub>2</sub> is fabricating the material as large scale crystallites.<sup>16</sup> Several calculations of the band structure of monolayer MoS<sub>2</sub> have been conducted.<sup>17–21</sup> Reducing the thickness of the material from bulk to a monolayer also increases the bandgap overall.<sup>22</sup> An increase of the band gap of MoS<sub>2</sub> from 1.29 eV to 1.9 eV was found by Mak *et al.*<sup>1</sup> It has been reported that with a fine control over the number of layers forming a MoS<sub>2</sub>, the work function of a surface may be tuned allowing for surfaces to be tuned for specific interfacing and the surface potential can be changed.<sup>23</sup> The electronic properties such as the band structure and exciton binding energies and the geometric properties of a

MoS<sub>2</sub> sample change when strain is introduced into a sample.<sup>17,24,25</sup> The properties of MoS<sub>2</sub> can also be changed through doping.<sup>19</sup>

Direct measurements of the band structure of MoS<sub>2</sub> are rare and difficult to perform. The reason is that photoelectron spectroscopy, as the method typically used for investigating the electronic structure of surfaces, probes several monolayers at a sample surface and in case of monolayer MoS<sub>2</sub> therefore the monolayer plus the top few layers of the substrate. The resulting spectra thus show the density of states (DOS) of the monolayer MoS<sub>2</sub> plus that of the substrate.<sup>25–28</sup> One of the few examples of measuring the DOS of monolayer MoS<sub>2</sub> are from Eknapakul *et al.* who determined the band structure of monolayer MoS<sub>2</sub> with intercalated potassium layers with angle resolved photoelectron spectroscopy (ARPES).<sup>5</sup> However, due to the presence of the K interlayers the results found through this work have to be considered to differ from monolayer MoS<sub>2</sub>. This situation leaves the literature of investigating MoS<sub>2</sub> monolayers deposited onto substrates with a situation that the electron spectrum of MoS<sub>2</sub> is known with a high degree of plausibility but not with spectra of MoS<sub>2</sub> only.

It is an intrinsic problem of all methods of photoelectron spectroscopy that in the of investigating monolayer materials deposited onto a substrate, that the contribution of the monolayer and the substrate cannot be separated unless the spectrum of the substrate covers an entirely different electron binding energy range compared to the monolayer material. The latter is usually not the case. This problem could only be overcome by applying an electron spectroscopy method which is sensitive to the outermost layer only such as metastable induced electron spectroscopy (MIES) or by applying a procedure in the data evaluation which allows to separate the contributions of the monolayer and the substrate. The disadvantage of MIES is that it would be sensitive only to the outer electronic structure of the monolayer and not to the overall monolayer. We thus have

<sup>a</sup> Flinders Institute for NanoScale Science and Technology, Flinders University, Adelaide, SA 5001, Australia. E-mail: gunther.andersson@flinders.edu.au; Tel: +61 8 82012309

<sup>b</sup> Flinders Microscopy and Microanalysis, College of Science and Engineering, Flinders University, Bedford Park, SA 5042, Australia

† Electronic supplementary information (ESI) available. See DOI: <https://doi.org/10.1039/d4lf00165f>



chosen in the present work a different route and applied a component analysis method for the data evaluation. The variation of the surface coverage with MoS<sub>2</sub> can be used as advantage in a component analysis because it introduces a variation in the contribution of the substrate and the monolayer to the spectra taken from various spots of the sample and allows for a mathematical separation of the spectral contributions of monolayer and substrate. The method developed in this work can in general be used for investigating any monolayer material deposited onto a substrate.

The aim of the present work is to determine experimentally the valence electron structure of monolayer MoS<sub>2</sub>. UV photoelectron spectroscopy (UPS) is applied, and the data are processed through component analysis separating the spectral contributions of the monolayer MoS<sub>2</sub> and that of the substrate. The data processing also allows to separate the spectra of monolayer and few layer MoS<sub>2</sub> showing the transition of the valence electron structure from the monolayer over the few layer to bulk MoS<sub>2</sub>. We have chosen a Si wafer with naturally oxidised SiO<sub>2</sub> as substrate. SiO<sub>2</sub> is known to interact only weakly with the MoS<sub>2</sub> monolayer<sup>29</sup> which we assume is holding also in the present case. In this way the valence electron structure of monolayer MoS<sub>2</sub> can be determined where the valence electron structure is only weakly modified through the interaction with the substrate. The combination of careful preparation of a sample containing mainly monolayer MoS<sub>2</sub> and some few layer MoS<sub>2</sub> with the component analysis of the electron spectra allows to show experimentally the change of the valence band edge with the thickness of MoS<sub>2</sub>.

## Experimental

### Materials and sample preparation

**Materials.** Monolayer MoS<sub>2</sub> crystals are grown on Si substrates with 300 nm thermal oxide using chemical vapor deposition (CVD) process according the method described by George *et al.*<sup>7</sup> The grown MoS<sub>2</sub> crystals were transferred onto Si (100) substrate from MTI corporation (B doped with a resistivity of 0.001–0.005 ohm cm) with native oxide using PMMA assisted transfer protocol.<sup>6</sup> For comparison a bulk MoS<sub>2</sub> sample from 2D Semiconductors (BLK-MOS2-SYN) was also investigated.

### X-ray photoelectron spectroscopy and ultraviolet photoelectron spectroscopy

The MoS<sub>2</sub> samples were investigated using XPS and UPS in an ultra-high vacuum (UHV) system built by SPECS (Berlin, Germany) which has a base pressure of a few 10<sup>-10</sup> mbar. The He\* and UV light (He I line) were generated in a two stage cold cathode gas discharge from MFM Analytical Systems (Claustal-Zellerfeld, Germany). A non-monochromatic X-ray source is used to generate Mg K $\alpha$  radiation. For detecting the emitted electrons a hemispherical Phoibos 100 energy analyser from SPECS (Berlin, Germany) was used. UPS and XPS were recorded at a pass energy of 10 eV and a bias of -10

V was applied to the samples for the UPS and metastable induced electron spectroscopy (MIES) measurements. The angle of UV and X-ray source radiation and the analyser are both 54° with respect to the surface normal of the sample. High resolution XP spectra were fitted with combined Gaussian–Lorentzian components and a correction for the Shirley background.<sup>30</sup> For quantification of relative intensities the cross sections calculated by Yeh have been used.<sup>31</sup>

For UPS the samples were irradiated with UV photons from the HeI line ( $h\nu = 21.2$  eV). The photons excite the valence electrons through the photoelectric effect. For HeI UPS the surface sensitivity is limited by the electron mean free path to the upper 2–3 nm of the sample.<sup>32</sup> The binding energy of the electrons in the sample is determined by eqn (1).

$$E_{\text{binding}} = 21.2 \text{ eV} - E_{\text{kinetic}} - \Phi_{\text{spec}} \quad (1)$$

where  $E_{\text{binding}}$  is the binding energy of the electrons in the sample,  $E_{\text{kinetic}}$  is the kinetic energy of the emitted electrons and  $\Phi_{\text{spec}}$  is the work function of the spectrometer. For XPS the binding energy is calculated in a similar way. The probing depth of XPS at this energy is about 6–7 nm, and slightly higher than in case of UPS due to the higher kinetic energy of the emitted electrons.<sup>32</sup>

MIES was applied at the same time as UPS. The MIE spectra have no significant features in the region up to 6 eV. The reason in the present case is that MoS<sub>2</sub> has states at low binding energy which favours the resonance ionisation (RI) followed by Auger neutralisation (AN) mechanism for the deexcitation of the metastable He atoms.<sup>33</sup>

While running UPS and MIES, the measurements were monitored for evidence of charging. As a routine, the measurements are conducted in a sequence of acquiring three spectra consecutively with the first two spectra consisting of single scans only. The samples are started to be exposed to UV photons and He\* just before the data acquisition is started. This is facilitated by keeping the valve between the UV and He\* source and the analysis chamber of the equipment closed until the data acquisition starts. In case the secondary onset of the measurements stays stable without showing a shift between the three measurements, charging of the sample during the measurements can reasonably be excluded. We also did not find charging of the MoS<sub>2</sub> during the XPS measurement.

### Scanning electron microscopy and auger electron spectroscopy

The MoS<sub>2</sub> on SiO<sub>2</sub> samples were analysed with a PHI710 Scanning Auger Nanoprobe (Flinders Microscopy and Microanalysis, Flinders University) with an electron energy of 1 keV. Auger electron spectroscopy (AES) is a similar spectroscopic technique to XPS. The sample is irradiated with an electron beam with a kinetic energy of the electrons from 1 to 25 keV which results in the excitation of electrons in the sample



leading to their emission. In the present work 10 keV electrons were used. The atom from which an electron is emitted is in an excited state which subsequently transits to the ground state leading to the emission of an Auger electron with an energy characteristic for the specific element. The emission of the electrons is detected with a detector with spatial resolution similar to that of the scanning electron microscope (SEM) allowing spatially resolved elemental mapping of the surface. AES and AEM can be combined in one instrument which is called Auger electron microscopy (AEM). AEM has an advantage over SEM in conjunction with energy-dispersive X-ray spectroscopy (EDX) due to the surface sensitivity of AEM.

### Heating procedure

Before applying electron spectroscopy, the samples were heated to 723 K.

### Measurement procedure

XPS and UPS were measured on nine different locations using a medium magnification lens mode with a diameter of the spot size for the analysis of 1.4 mm. This allows for applying a component analysis to separate the components in UPS the spectra related to the various thickness of MoS<sub>2</sub> and the substrate. The central spot is located approximately in the middle of the MoS<sub>2</sub> shown in Fig. S1†. The other nine spots are located +2 mm or -2 mm to the left and right and top and bottom of the central spot. As an example, the spot (x, z) +2/-2 is located 2 mm above and 2 mm to the left of the central spot.

### SVD analysis

A mathematical algorithm known as singular value decomposition (SVD) is used to analyse a series of UP spectra. The details of the procedure can be found in literature.<sup>34–36</sup> A summary is provided in the ESI.† The SVD procedure results in reference spectra which are used to reproduce the measured UP spectra as linear combination. The reference spectra represent spectra of a surface with a specific composition and electronic structure.

### Raman spectroscopy

Raman spectra were acquired using a WITec alpha 300 R Raman microscope at an excitation laser wavelength of 532 nm ( $\leq 5$  mW) with a  $\times 40$  objective (numerical aperture 0.60). A minimum of 15 Raman spectra were recorded per sample at approximately 5 separate locations within each sample. Typical integrations times were 10–30 s for 2–3 accumulations per spectrum.

## Results and discussion

### SEM imaging

In Fig. 1 a SEM image of the central part of the sample is shown. Triangular shaped features with medium grey scale brightness can be identified as thin MoS<sub>2</sub> crystallites with the

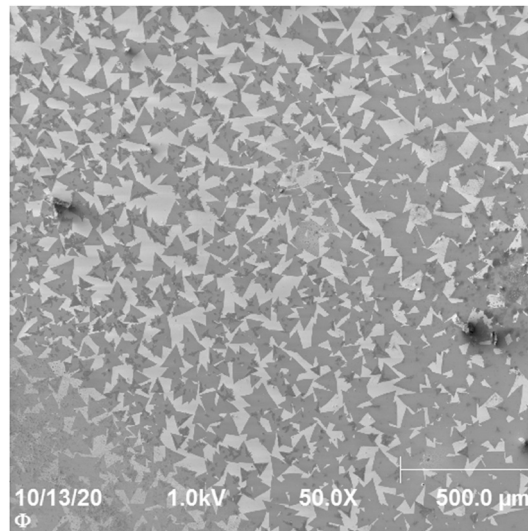


**Fig. 1** SEM image of the central area of the sample shown in Fig. S1†. The dark grey triangular shaped areas are the monolayer MoS<sub>2</sub> crystallites. The crystallites show a small degree of overlap. The relative fraction of the sample surface formed by the substrate, monolayer and few layer MoS<sub>2</sub> is provided in Table 1.

help of Auger microscopy and Raman spectroscopy (see Fig. S2 and S3 in the ESI†). Between the grey triangle areas lighter grey areas can be seen which is the uncovered Si wafer used as substrate. Additionally, some darker areas with overlap between the triangular crystallites can be identified and some dark areas with arbitrary shape. The latter will be identified below as contamination. The area analysis from Fig. 1 is shown in Table 1 with single MoS<sub>2</sub> sheets covering 61.4% of the surface, thicker MoS<sub>2</sub> covering 0.7%, contaminations covering 0.8% and the substrate representing 30.7% of the surface. The analysis of the coverage was done by a grey scale histogram analysis of the SEM image.

Fig. S1† shows an optical image of the MoS<sub>2</sub>. In Fig. 2 examples of key positions chosen to conduct Raman spectroscopy for evaluating the structural properties of the MoS<sub>2</sub> are shown. The respective Raman spectra are displayed adjacent to the indicated positions. The optical image itself appears to have triangular crystalline structures which corresponds to the expected shape of MoS<sub>2</sub> crystallites.<sup>10</sup>

The first region within the triangular crystalline shape appeared to be MoS<sub>2</sub> with peaks at 384.8 and 404.5 cm<sup>-1</sup> representing the E<sub>2g</sub><sup>1</sup> and A<sub>1g</sub> modes, respectively. The separation of these peaks (19.4 ± 0.5 cm<sup>-1</sup>) combined with the high intensity of the silicon peak at 520 cm<sup>-1</sup> indicates monolayer MoS<sub>2</sub> in this region.<sup>29</sup> The peak separation of 19.7

**Table 1** Coverage of the surface and fraction of coverage

Species	Fraction area [%]
Substrate (light grey), silicon wafer	30.7
MoS <sub>2</sub> , thin (medium light grey)	61.4
MoS <sub>2</sub> , thick (medium dark grey)	0.7
Contamination (dark grey)	0.8



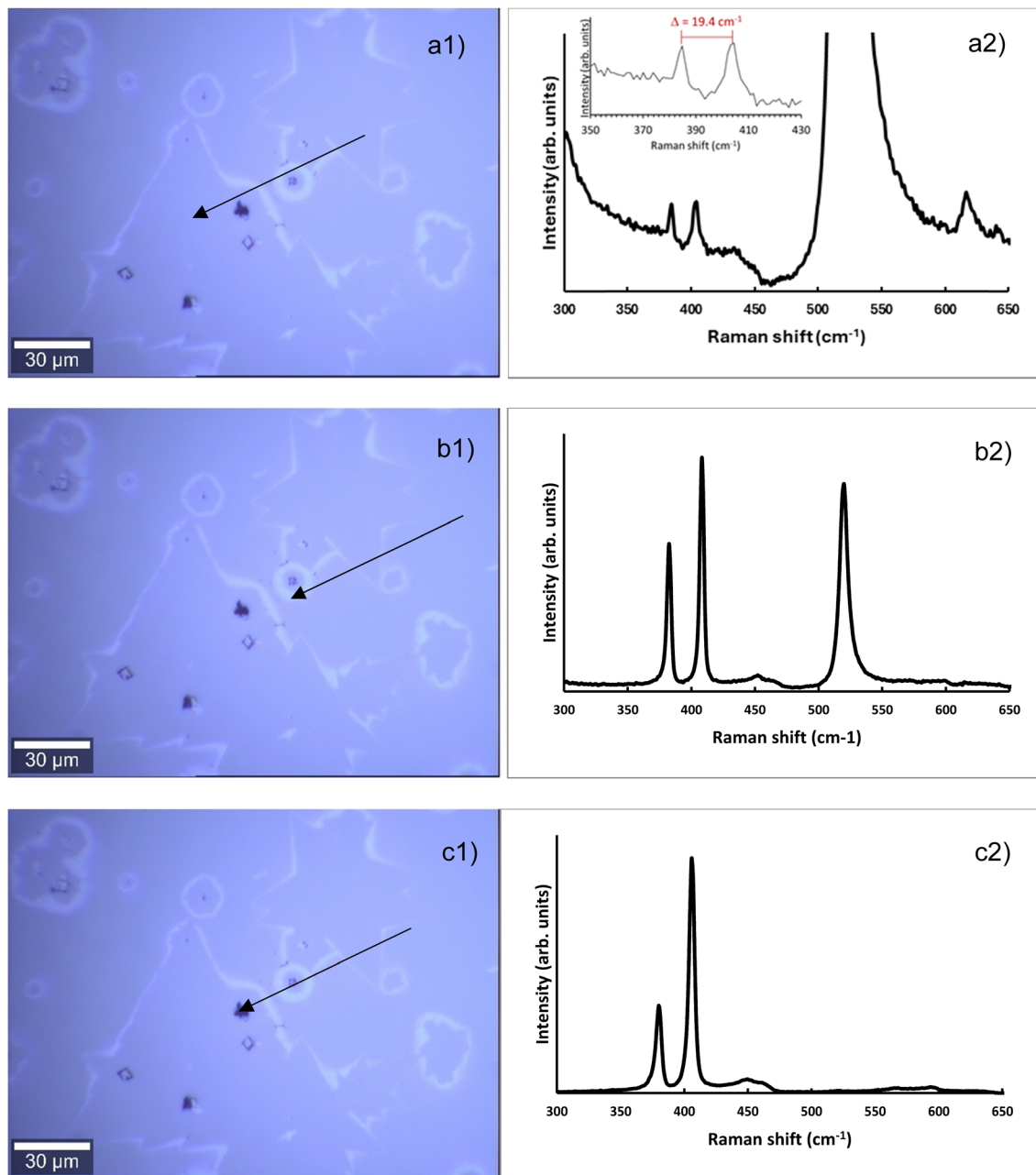


Fig. 2 Optical images (a1–c1) and Raman spectra (a2–c2) of specific areas on the optical image. In a1 an inset with the  $E_{2g}^1$  and  $A_{1g}$  modes are shown. In a2 an inset is shown with the separation of the  $E_{2g}^1$  and  $A_{1g}$  modes.

$\text{cm}^{-1}$  is between those found for monolayer  $\text{MoS}_2$  on  $\text{Al}_2\text{O}_3$  ( $18 \text{ cm}^{-1}$ ) and Au ( $21 \text{ cm}^{-1}$ ) were for the first substrate tensile strain and for the second compressive strain has been reported.<sup>37</sup> This finding is supporting the assumption that  $\text{SiO}_2$  as substrate used here results only in a weak interaction between the substrate and the  $\text{MoS}_2$  monolayer. The second location, a white cloudlike region, still has  $\text{MoS}_2$ , however the reduced silicon peak intensity, relative to the  $\text{MoS}_2$  peaks, indicates a higher  $\text{MoS}_2$  concentration. The  $\text{MoS}_2$  peaks are situated at  $382.5 \text{ cm}^{-1}$  and  $408.5 \text{ cm}^{-1}$  and are separated by  $26 \text{ cm}^{-1}$ . This separation combined with the higher  $\text{MoS}_2$  concentration than the monolayer indicates multilayer  $\text{MoS}_2$ .<sup>29,38</sup> The last region which

is a dark black spot on the optical image possesses high intensity  $\text{MoS}_2$  peaks at  $380.0 \text{ cm}^{-1}$  and  $406.0 \text{ cm}^{-1}$  with no visible silicon peaks. The  $\text{MoS}_2$  is thus thick enough to obstruct the detection of the silicon substrate and is classified as bulk  $\text{MoS}_2$ .

For better identifying the chemical nature of the crystallites AEM was applied. In the ESI† Fig. S2a shows SEM images indicating the position of the spots from which Auger spectra were taken with the latter shown in Fig. S2b.† The triangular shaped features with medium grey scale brightness can be identified as thin  $\text{MoS}_2$  crystallites. Fig. S2a† shows an SEM image of a similar sample with a single triangle in position 5 identified by AES as having very low Mo and S content being



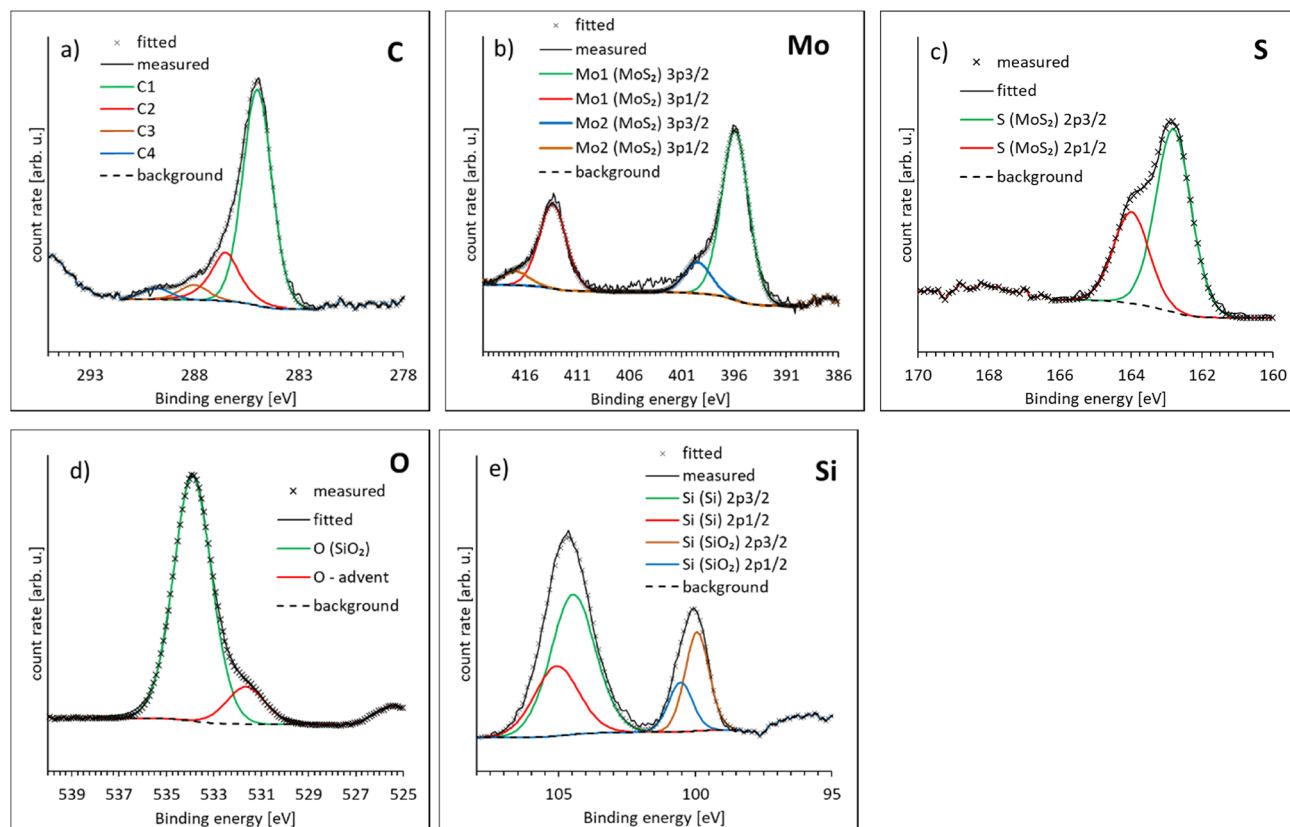


**Fig. 3** XPS spectra of a) C1s, b) Mo 3p, c) S 2p, d) O 1s, and e) Si 2p. The measured spectra are shown together with the fit of Shirley background and the spectral components.

linked to monolayer MoS<sub>2</sub>. The Auger spectra clearly identify that the deposited triangular shaped material in MoS<sub>2</sub>.

In the ESI† in Fig. S3 Raman spectra of one of the triangular crystallites are shown. From the Raman spectra the vast majority of the area of the triangular crystals can be identified as monolayer MoS<sub>2</sub> based on the separation of the E<sub>2g</sub><sup>1</sup> and A<sub>1g</sub> modes.<sup>29</sup> A small fraction of the crystallite area formed is few layer MoS<sub>2</sub>.

### XPS analysis

In Fig. 3 the high resolution XPS spectra of the sample are shown with the binding energies of all components found

listed in Table 2. In Fig. 3a the C1s spectrum is shown. The components are C1 at 285 (sp<sup>3</sup> C–C), C2 at 286.5 ± 0.2 eV assigned to C–O (ref. 39) or C–OH (ref. 40) or similar bonds, C3 at 288.0 ± 0.2 eV assigned to C=O (ref. 40) and C4 at 289.8 ± 0.2 eV assigned to C(O)OH.<sup>40</sup> All these carbon species are adventitious carbon. Their specific nature is not relevant for the present work. In Fig. 3b the Mo 3p doublet is shown with the 3p<sub>3/2</sub> peak at 395.9 ± 0.2 eV which can be identified as Mo in MoS<sub>2</sub>.<sup>41</sup> A small peak for MoO<sub>3</sub> was found at 399.5 ± 0.2 eV (ref. 41) with 16% of the overall Mo intensity. This Mo peak is not the main peak for Mo in XPS. However, the main Mo 3d<sub>5/2</sub> peak at around 228 eV is overlapping with the S 2s peak and for this reason could not be used for the data

**Table 2** Binding energies XPS spectra and relative intensities averaged over all nine analysed spots

Component	Chemical species	Binding energy ± 0.2 [eV]	Rel. intensities [%]
C1–C1s	C–C sp <sup>3</sup> , adventitious	285	13.2 ± 0.3
C2–C1s	C–O or C–OH, <sup>39</sup> adventitious	286.5	3.3 ± 0.3
C3–C1s	C=O, <sup>40</sup> adventitious	288.0	0.9 ± 0.3
C4–C1s	C(O)OH, <sup>40</sup> adventitious	289.8	0.7 ± 0.3
Mo	MoS <sub>2</sub> (ref. 41)	395.9	3.4 ± 0.1
Mo	MoO <sub>3</sub> (ref. 41)	399.5	0.6 ± 0.1
S	MoS <sub>2</sub> (ref. 42)	162.8	7.0 ± 0.1
O1	SiO <sub>2</sub> (ref. 43)	533.9	36.4 ± 0.4
O2	OH, adventitious	531.7	5.6 ± 0.4
Si1	Si (ref. 43)	99.9	8.0 ± 0.2
Si2	SiO <sub>2</sub> (ref. 43)	104.5	20.9 ± 0.2



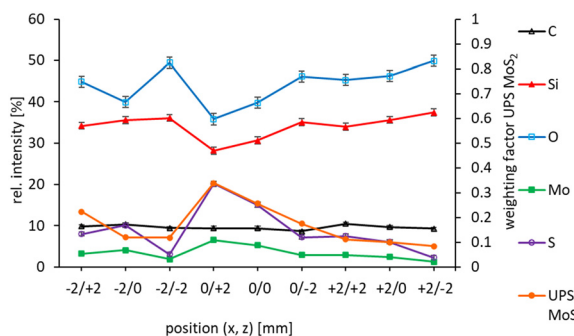


Fig. 4 Relative intensities of XPS for the nine different spots versus their location.

analysis. In Fig. 3c the S 2p doublet is shown with the  $2p_{3/2}$  peak at  $162.8 \pm 0.2$  eV which can be identified as Mo in  $\text{MoS}_2$ .<sup>42</sup> In Fig. 3c the O 1s spectrum with one component O1 at  $533.9 \pm 0.2$  eV and a second small component at  $531.7 \pm 0.2$  eV. The first is O of  $\text{SiO}_2$  (ref. 43) while the latter is probably adventitious OH. In Fig. 3d the Si 2p region with two doublets are shown. The  $2p_{3/2}$  peak of one doublet is found at  $99.9 \pm 0.2$  eV and can be identified as Si while the second doublet is at  $104.5 \pm 0.2$  eV which can be identified as  $\text{SiO}_2$ .<sup>43</sup> The ratio of Mo to S based on the relative intensities shown in Table 2 is  $0.49 \pm 0.02$  thus corresponds to the stoichiometric ratio of the two elements.

The combined relative intensities of  $\text{MoS}_2$  of 12.1% are compatible with a  $\text{MoS}_2$  layer thickness of approximately 4 Å at a coverage of 60%.

In Fig. 4 the relative intensities of the elements detected with XPS for all nine spots are shown. It can be seen that the coverage with  $\text{MoS}_2$  is highest in the centre of the sample along the  $x$ -axis, *i.e.* at  $x = 0$ .

### UPS analysis

In Fig. 5 the UP spectra of all nine spots analysed are shown. The components of the series of the nine spectra were analysed with SVD. SVD has been proven to be a powerful data analysis tool when the various components of a sample

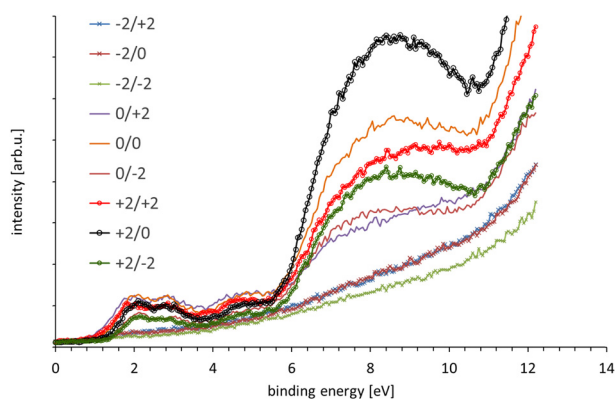


Fig. 5 UP spectra of all nine analysed spots across the sample.

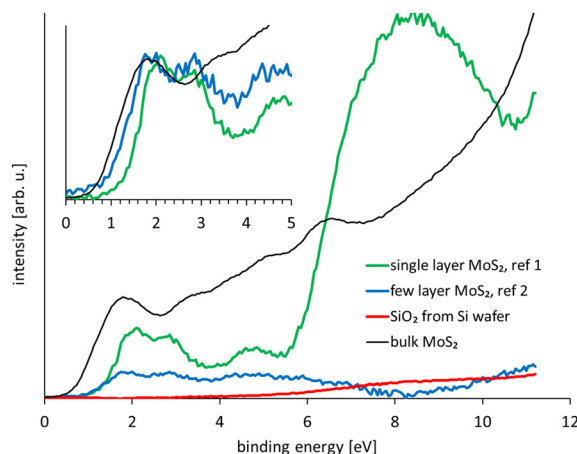


Fig. 6 Spectra of the components forming the  $\text{MoS}_2/\text{Si}/\text{SiO}_2$  sample: the monolayer  $\text{MoS}_2$ , few layer  $\text{MoS}_2$  and the  $\text{Si}/\text{SiO}_2$  substrate. For reference a spectrum of bulk  $\text{MoS}_2$  is shown. In the inset the onset of the VB are shown. In the inset spectra are scaled such that they have the same intensity at their first maximum around 1 to 1.5 eV.

cannot physically be separated for the process of the analysis. SVD has been successfully applied to separate in electron spectroscopy the various components at liquid surfaces and solid surfaces,<sup>44</sup> clusters on surfaces<sup>45</sup> and interfaces in organic electronics.<sup>46</sup>

The reference spectra resulting from the SVD analysis are shown in Fig. 6 and the weighting factors for the reference spectra are shown in Fig. 7. These reference spectra represent the components forming the sample and the weighting factor the fraction of their contribution to the measured spectra. The spectrum of bulk  $\text{MoS}_2$  is also shown. Two reference spectra were found representing  $\text{MoS}_2$ . The first reference spectrum is assigned to single monolayer of  $\text{MoS}_2$ . The reason for this assignment is that the spectrum shows the characteristic structure of  $\text{MoS}_2$  similar to the bulk  $\text{MoS}_2$  in the region 6 eV binding energy. Additionally, this reference spectrum shows a broad distribution between 6 and 10 eV which is characteristic for  $\text{SiO}_2$ . Thus the first reference spectrum is a combination of the spectrum from single layer

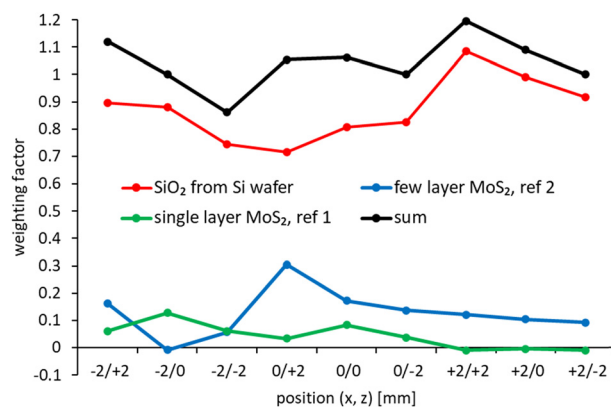


Fig. 7 Weighting factors for the SVD component analysis.



MoS<sub>2</sub> and SiO<sub>2</sub> with the later contributing only intensity at binding energies >6 eV. The part of the spectrum at <6 eV thus can be assigned exclusively to monolayer MoS<sub>2</sub>. The second reference spectrum is also assigned to MoS<sub>2</sub>. In contrast to the first reference spectrum it does not show the broad SiO<sub>2</sub> feature between 6 and 10 eV. The second reference spectrum is assigned to stacking of monolayer MoS<sub>2</sub> forming bilayers as it could be identified from Fig. 1. The valence electron cut-off is at a binding energy between monolayer and bulk MoS<sub>2</sub>. This MoS<sub>2</sub> species is referred here to “few” layer. Although it is likely that this species is a double layer, we refer here to “few” because we cannot provide unambiguous evidence for a double layer species. The third reference spectrum is assigned to SiO<sub>2</sub> showing only the broad distribution between 6 and 10 eV characteristic for SiO<sub>2</sub>.

In Fig. 4 the sum of the weighting factors for the first and second MoS<sub>2</sub> spectra are shown. It can be seen that the sum of the MoS<sub>2</sub> weighting factors follows closely the relative intensities of Mo and S in XPS confirming the assignment of reference spectra 1 and 2 to MoS<sub>2</sub>.

The valence band (VB) cut-off for bulk MoS<sub>2</sub> is found at  $0.64 \pm 0.05$  eV as can be seen in Fig. S3 which is similar to what was found by Timpel *et al.* for annealed MoS<sub>2</sub>.<sup>2</sup> Comparing the VB cut-off of both reference spectra with that of bulk MoS<sub>2</sub> it can be seen in the inset of Fig. 6 that the single layer MoS<sub>2</sub> is shifted by about 0.6 eV to higher binding energies of 1.26 eV and the few layer MoS<sub>2</sub> by about 0.25 eV to 0.89 eV; the respective VB cut-offs are also shown in Fig. S3.†

The shift in the VB cut-off is consistent with the increase in band gap found by Mak *et al.* who found an increase in band gap from 6 to 1 monolayer MoS<sub>2</sub> of 0.5 eV.<sup>1</sup> In case the conduction band (CB) cut-off does not move at the same time to lower energies, the band gap of the single and double layer MoS<sub>2</sub> has increased. Mak *et al.* found a shift in band gap of almost the same amount as found here for the change of the valence band edge for the transition from bulk to monolayer MoS<sub>2</sub>, and it could be hypothesised that the CB position does not change at the same time. However, computer calculations show a decrease in the CB position with increasing number of MoS<sub>2</sub> layers which also would contribute to a decrease of the band gap of MoS<sub>2</sub> with increasing number of layers. It should be noted that it would be needed to measure the position of the conduction band for MoS<sub>2</sub> with a variation of the number of layers, which should be possible with a technique like inverse photoemission spectroscopy.<sup>28</sup>

The VB cut-off found by Eknapul *et al.* of MoS<sub>2</sub> with an interlayer of K is found at 1.89 eV which is larger than what is found in the present work. The reason might be the interaction of MoS<sub>2</sub> with the K interlayer. Interaction with substrates had been found by Park *et al.* who reported a VB cut-off for MoS<sub>2</sub> on SiO<sub>2</sub> of 1.81 eV and on Au of 1.30 eV.<sup>27</sup> Park *et al.* have used the same preparation as in the present work. It is unclear why the VB cut-off reported by these authors is different to our work.

## Conclusion

We have determined the valence electron structure of monolayer MoS<sub>2</sub> deposited onto SiO<sub>2</sub> with UPS. Component analysis of UP spectra acquired in a spatially resolved mode separating various areas of the sample with mm resolution in combination with SEM and spatially resolved XPS have been used to separate the components in the UP spectra. The valence electron of MoS<sub>2</sub> only weakly interacting with the SiO<sub>2</sub> substrate shows a VB cut-off which is at 0.6 eV higher binding energy than bulk MoS<sub>2</sub>. The double layer shows an increase in the binding energy of the cut-off of 0.25 eV.

## Data availability

All data supporting this article have been included either in the main manuscript or in the ESI.†

## Conflicts of interest

There is no conflict of interest to be reported.

## Acknowledgements

This work was supported by the College of Science and Engineering at Flinders University and by a grant of the Australian Research Council (LE0989068). The authors would like to thank Anthony George and Andrey Turchanin of the Institute of Physical Chemistry at the Friedrich Schiller University in Jena (Germany) for providing the monolayer MoS<sub>2</sub> samples. The authors acknowledge the facilities, and the scientific and technical assistance, of Microscopy Australia (formerly known as AMMRF) and the Australian National Fabrication Facility (ANFF) at Flinders University. The authors would also like to acknowledge the expertise and support provided by Flinders Microscopy and Microanalysis (FMMA).

## References

- 1 K. F. Mak, C. Lee, J. Hone, J. Shan and T. F. Heinz, Atomically Thin MoS<sub>2</sub>: A New Direct-Gap Semiconductor, *Phys. Rev. Lett.*, 2010, **105**, 136805.
- 2 M. Timpel, G. Ligorio, A. Ghiami, L. Gavioli, E. Cavaliere, A. Chiappini, F. Rossi, L. Pasquali, F. Gärisch, E. J. W. List-Kratochvil, P. Nozar, A. Quaranta, R. Verucchi and M. V. Nardi, 2D-MoS<sub>2</sub> goes 3D: transferring optoelectronic properties of 2D MoS<sub>2</sub> to a large-area thin film, *npj 2D Mater. Appl.*, 2021, **5**, 64.
- 3 J. Kang, L. Zhang and S.-H. Wei, A Unified Understanding of the Thickness-Dependent Bandgap Transition in Hexagonal Two-Dimensional Semiconductors, *J. Phys. Chem. Lett.*, 2016, **7**, 597–602.
- 4 L. Zhang and A. Zunger, Evolution of Electronic Structure as a Function of Layer Thickness in Group-VIB Transition Metal Dichalcogenides: Emergence of Localization Prototypes, *Nano Lett.*, 2015, **15**, 949–957.



- 5 T. Eknapakul, P. D. C. King, M. Asakawa, P. Buaphet, R. H. He, S. K. Mo, H. Takagi, K. M. Shen, F. Baumberger, T. Sasagawa, S. Jungthawan and W. Meevasana, Electronic Structure of a Quasi-Freestanding MoS<sub>2</sub> Monolayer, *Nano Lett.*, 2014, **14**, 1312–1316.
- 6 A. Winter, A. George, C. Neumann, Z. Tang, M. J. Mohn, J. Biskupek, N. Masurkar, A. L. M. Reddy, T. Weimann, U. Hübner, U. Kaiser and A. Turchanin, Lateral heterostructures of two-dimensional materials by electron-beam induced stitching, *Carbon*, 2018, **128**, 106–116.
- 7 A. George, C. Neumann, D. Kaiser, R. Mupparapu, T. Lehnert, U. Hübner, Z. Tang, A. Winter, U. Kaiser, I. Staude and A. Turchanin, Controlled growth of transition metal dichalcogenide monolayers using Knudsen-type effusion cells for the precursors, *JPhys Mater.*, 2019, **2**, 016001.
- 8 G. U. Von Oertzen, S. L. Harmer and W. M. Skinner, XPS and ab initio calculation of surface states of sulfide minerals: pyrite, chalcopyrite and molybdenite, *Mol. Simul.*, 2006, **32**, 1207–1212.
- 9 W. Choi, N. Choudhary, G. H. Han, J. Park, D. Akinwande and Y. H. Lee, Recent development of two-dimensional transition metal dichalcogenides and their applications, *Mater. Today*, 2017, **20**, 116–130.
- 10 X. Yang and B. Li, Monolayer MoS<sub>2</sub> for nanoscale photonics, *Nanophotonics*, 2020, **9**, 1557–1577.
- 11 F. G. Aras, A. Yilmaz, H. G. Tasdelen, A. Ozden, F. Ay, N. K. Perkgoz and A. Yeltik, A review on recent advances of chemical vapor deposition technique for monolayer transition metal dichalcogenides (MX<sub>2</sub>: Mo, W; S, Se, Te), *Mater. Sci. Semicond. Process.*, 2022, **148**, 106829.
- 12 I. Paradisanos, S. Shree, A. George, N. Leisgang, C. Robert, K. Watanabe, T. Taniguchi, R. J. Warburton, A. Turchanin, X. Marie, I. C. Gerber and B. Urbaszek, Controlling interlayer excitons in MoS<sub>2</sub> layers grown by chemical vapor deposition, *Nat. Commun.*, 2020, **11**, 2391.
- 13 T.-X. Huang, X. Cong, S.-S. Wu, K.-Q. Lin, X. Yao, Y.-H. He, J.-B. Wu, Y.-F. Bao, S.-C. Huang, X. Wang, P.-H. Tan and B. Ren, Probing the edge-related properties of atomically thin MoS<sub>2</sub> at nanoscale, *Nat. Commun.*, 2019, **10**, 5544.
- 14 J. Theerthagiri, R. A. Senthil, B. Senthilkumar, A. Reddy Polu, J. Madhavan and M. Ashokkumar, Recent advances in MoS<sub>2</sub> nanostructured materials for energy and environmental applications – A review, *J. Solid State Chem.*, 2017, **252**, 43–71.
- 15 U. Yadav, H. Mishra, V. Singh, S. Kashyap, A. Srivastava, S. Yadav and P. S. Saxena, Enhanced Osteogenesis by Molybdenum Disulfide Nanosheet Reinforced Hydroxyapatite Nanocomposite Scaffolds, *ACS Biomater. Sci. Eng.*, 2019, **5**, 4511–4521.
- 16 Y. Liu and F. Gu, A wafer-scale synthesis of monolayer MoS<sub>2</sub> and their field-effect transistors toward practical applications, *Nanoscale Adv.*, 2021, **3**, 2117–2138.
- 17 H. L. Zhu, C. J. Zhou, X. J. Huang, X. L. Wang, H. Z. Xu, Y. Lin, W. H. Yang, Y. P. Wu, W. Lin and F. Guo, Evolution of band structures in MoS<sub>2</sub>-based homo- and heterobilayers, *J. Phys. D: Appl. Phys.*, 2016, **49**, 065304.
- 18 M.-T. Wu, J.-W. Fan, K.-T. Chen, S.-T. Chang and C.-Y. Lin, Band Structure and Effective Mass in Monolayer MoS<sub>2</sub>, *J. Nanosci. Nanotechnol.*, 2015, **15**, 9151–9157.
- 19 C. Hu, C. Yuan, A. Hong, M. Guo, T. Yu and X. Luo, Work function variation of monolayer MoS<sub>2</sub> by nitrogen-doping, *Appl. Phys. Lett.*, 2018, **113**, 041602.
- 20 W. Zhao, J. Pan, Y. Fang, X. Che, D. Wang, K. Bu and F. Huang, Metastable MoS<sub>2</sub>: Crystal Structure, Electronic Band Structure, Synthetic Approach and Intriguing Physical Properties, *Chem. – Eur. J.*, 2018, **24**, 15942–15954.
- 21 L. Szulakowska, M. Bieniek and P. Hawrylak, Electronic structure, magnetoexcitons and valley polarized electron gas in 2D crystals, *Solid-State Electron.*, 2019, **155**, 105–110.
- 22 G. Fugallo, P. Cudazzo, M. Gatti and F. Sottile, Exciton band structure of molybdenum disulfide: from monolayer to bulk, *Electron. Struct.*, 2021, **3**, 014005.
- 23 B. J. Robinson, C. E. Giusca, Y. T. Gonzalez, N. D. Kay, O. Kazakova and O. V. Kolosov, Structural, optical and electrostatic properties of single and few-layers MoS<sub>2</sub>: effect of substrate, *2D Mater.*, 2015, **2**, 015005.
- 24 S. Aas and C. Bulutay, Geometric band properties in strained monolayer transition metal dichalcogenides using simple band structures, *J. Appl. Phys.*, 2019, **126**, 115701.
- 25 S. Ulstrup, A. G. Čabo, J. A. Miwa, J. M. Riley, S. S. Grønborg, J. C. Johannsen, C. Cacho, O. Alexander, R. T. Chapman, E. Springate, M. Bianchi, M. Dendzik, J. V. Lauritsen, P. D. C. King and P. Hofmann, Ultrafast Band Structure Control of a Two-Dimensional Heterostructure, *ACS Nano*, 2016, **10**, 6315–6322.
- 26 F. Bussolotti, J. Yang, H. Kawai, C. P. Y. Wong and K. E. J. Goh, Impact of S-Vacancies on the Charge Injection Barrier at the Electrical Contact with the MoS<sub>2</sub> Monolayer, *ACS Nano*, 2021, **15**, 2686–2697.
- 27 S. Park, T. Schultz, D. Shin, N. Mutz, A. Aljarb, H. S. Kang, C.-H. Lee, L.-J. Li, X. Xu, V. Tung, E. J. W. List-Kratochvil, S. Blumstengel, P. Amsalem and N. Koch, The Schottky–Mott Rule Expanded for Two-Dimensional Semiconductors: Influence of Substrate Dielectric Screening, *ACS Nano*, 2021, **15**, 14794–14803.
- 28 S. Park, N. Mutz, T. Schultz, S. Blumstengel, A. Han, A. Aljarb, L.-J. Li, E. J. W. List-Kratochvil, P. Amsalem and N. Koch, Direct determination of monolayer MoS<sub>2</sub> and WSe<sub>2</sub> exciton binding energies on insulating and metallic substrates, *2D Mater.*, 2018, **5**, 025003.
- 29 C. Lee, H. Yan, L. E. Brus, T. F. Heinz, J. Hone and S. Ryu, Anomalous Lattice Vibrations of Single- and Few-Layer MoS<sub>2</sub>, *ACS Nano*, 2010, **4**, 2695–2700.
- 30 D. A. Shirley, High -Resolution X-Ray Photoemission Spectrum of the Valence Bands of Gold, *Phys. Rev. B: Solid State*, 1972, **5**, 4709–4714.
- 31 J. J. Yeh and I. Lindau, Atomic subshell photoionization cross sections and asymmetry parameters:  $1 \leq Z \leq 103$ , *At. Data Nucl. Data Tables*, 1985, **32**, 1–155.
- 32 M. P. Seah and W. A. Dench, Quantitative electron spectroscopy of surfaces: A standard data base for electron inelastic mean free paths in solids, *Surf. Interface Anal.*, 1979, **1**, 2–11.



- 33 H. Morgner, The quantitative characterization of liquid and solid surfaces with metastable helium atoms, in *Physics of Electronic and Atomic Collisions*, ed. Y. Itikawa, K. Okuno, A. H. Tanaka, A. Yagishita and M. Matsuzawa, 2000, vol. 500, pp. 687–698.
- 34 H. Morgner, The Characterization of Liquid and Solid Surfaces with Metastable Helium Atoms, in *Advances In Atomic, Molecular, and Optical Physics*, ed. B. Benjamin and W. Herbert, Academic Press, 2000, vol. 42, pp. 387–488.
- 35 A. Berlich, Y. C. Liu and H. Morgner, Evaporation of Ni and Carbon Containing Species onto NiO/Ni as Case Study for Metal Support Catalysts Investigated by Metastable Induced Electron Spectroscopy (MIES), *Radiat. Phys. Chem.*, 2005, **74**, 201–209.
- 36 J. Oberbrodthage, Determination of a solute electron energy spectrum not accessible experimentally by means of Singular Value Decomposition, *J. Electron Spectrosc. Relat. Phenom.*, 2000, **107**, 231–238.
- 37 S. E. Panasci, E. Schilirò, G. Greco, M. Cannas, F. M. Gelardi, S. Agnello, F. Roccaforte and F. Giannazzo, Strain, Doping, and Electronic Transport of Large Area Monolayer MoS<sub>2</sub> Exfoliated on Gold and Transferred to an Insulating Substrate, *ACS Appl. Mater. Interfaces*, 2021, **13**, 31248–31259.
- 38 S. Mignuzzi, A. J. Pollard, N. Bonini, B. Brennan, I. S. Gilmore, M. A. Pimenta, D. Richards and D. Roy, Effect of disorder on Raman scattering of single-layer MoS<sub>2</sub>, *Phys. Rev. B: Condens. Matter Mater. Phys.*, 2015, **91**, 195411.
- 39 S. Rella, E. Mazzotta, A. Caroli, M. De Luca, C. Bucci and C. Malitesta, Investigation of polydopamine coatings by X-ray Photoelectron Spectroscopy as an effective tool for improving biomolecule conjugation, *Appl. Surf. Sci.*, 2018, **447**, 31–39.
- 40 D. Yang, A. Velamakanni, G. Bozoklu, S. Park, M. Stoller, R. D. Piner, S. Stankovich, I. Jung, D. A. Field, C. A. Ventrice and R. S. Ruoff, Chemical analysis of graphene oxide films after heat and chemical treatments by X-ray photoelectron and Micro-Raman spectroscopy, *Carbon*, 2009, **47**, 145–152.
- 41 T. A. Patterson, J. C. Carver, D. E. Leyden and D. M. Hercules, A surface study of cobalt-molybdena-alumina catalysts using x-ray photoelectron spectroscopy, *J. Phys. Chem.*, 1976, **80**, 1700–1708.
- 42 N. H. Turner and A. M. Single, Determination of peak positions and areas from wide-scan XPS spectra, *Surf. Interface Anal.*, 1990, **15**, 215–222.
- 43 M. H. Kibel and P. W. Leech, X-ray Photoelectron Spectroscopy Study of Optical Waveguide Glasses, *Surf. Interface Anal.*, 1996, **24**, 605–610.
- 44 B. Heinz and H. Morgner, Surface characterization by means of quantitative evaluation of MIES data, *J. Electron Spectrosc. Relat. Phenom.*, 1998, **96**, 83–95.
- 45 G. Krishnan, H. S. Al Qahtani, J. Li, Y. Yin, N. Eom, V. B. Golovko, G. F. Metha and G. G. Andersson, Investigation of Ligand-Stabilized Gold Clusters on Defect-Rich Titania, *J. Phys. Chem. C*, 2017, **121**, 28007–28016.
- 46 A. R. Alghamdi, J. M. Bjuggren, X. Pan, M. R. Andersson and G. G. Andersson, Dipole Formation at Active Materials/P(NDI3N-T-Br) Interface in Organic-Based Photovoltaic, *Macromol. Mater. Eng.*, 2022, **307**, 2200303.

